Spin-to-Charge Conversion in Bi Films and Bi/Ag Bilayers

Di Yue, Weiwei Lin, Jiajia Li, Xiaofeng Jin, and C. L. Chien

Phys. Rev. Lett. **121**, 037201 — Published 16 July 2018

DOI: 10.1103/PhysRevLett.121.037201

Spin-to-Charge Conversion in Bi Films and Bi/Ag Bilayers

Di Yue,[1,2,3] Weiwei Lin,[1] Jiajia Li,[2,3] Xiaofeng Jin,[2,3] and C. L. Chien[1,4]

[1] *Department of Physics and Astronomy, Johns Hopkins University, Baltimore, Maryland 21218, USA*
[2] *State Key Laboratory of Surface Physics and Department of Physics, Fudan University, Shanghai 200433, China*
[3] *Collaborative Innovation Center of Advanced Microstructures, Fudan University, Shanghai 200433, China*
[4] *Institute of Physics, Academia Sinica, Taipei 11529, Taiwan*

(Dated: June 25, 2018)

Thermally-injected pure spin current phenomena have been investigated in $Bi/Y_3Fe_5O_{12}$ and $Bi/Ag/Y_3Fe_5O_{12}$ structures at room temperature. We show that although pure spin current has been injected into the Bi layer and the Bi/Ag bilayer, there is little detectable signal of spin-to-charge conversion, except the distinctive Nernst signal from the Bi layer, in sharp contrast to the inverse Rashba-Edelstein effect claimed in these systems.

Pure spin current phenomena and devices are new advents in spintronics. With a flow of angular momentum without accompanying charge currents, a pure spin current generates no Oersted field and the least Joule heating, thus highly advantageous. To generate a spin current, one may employ spin Hall effect (SHE) [1–3], spin pumping (SP) [4–9] at ferromagnetic resonance (FMR), lateral spin valve (LSV) [10, 11], or longitudinal spin Seebeck effect (LSSE) [12–14]. Once generated, a pure spin current cannot be detected by the usual electrical means except indirectly via inverse spin Hall effect (ISHE) [3, 7, 15] using a heavy metal with strong spin-orbit coupling (SOC) [16–18]. The spin-to-charge conversion results a charge current, $\boldsymbol{j}_C = \theta_{SH}[2e/\hbar]\boldsymbol{j}_S \times \boldsymbol{\sigma}$, in a direction perpendicular to both the spin current $\boldsymbol{j}_S$ and the spin index $\boldsymbol{\sigma}$, where θ_{SH} is the spin Hall angle that measures the conversion efficiency. Usually, one detects the resulting DC voltage, namely the ISHE voltage, as the evidence of spin-to-charge conversion. Thus, one must carefully ascertain that the measured voltage is indeed due to spin-to-charge conversion and not those from a host of parasitic effects.

Bismuth (Bi) is the heaviest non-radioactive element in the Periodic Table. It is natural to exploit the large SOC in Bi metal [19, 20] and Bi-containing materials [21–32] for spin current phenomena. However, there are already conflicting results even in Bi metal and bilayers. In SP experiments on Bi/permalloy at room temperature [19], using the ferromagnetic (FM) metal permalloy ($Ni_{81}Fe_{19}$) as the spin injector, the transverse DC voltage measured at FMR has been taken as evidence of spin-to-charge conversion, resulting in a substantial $\theta_{SH} = 0.02$ for Bi. However, SP experiments on Bi/YIG [20], using the ferrimagnetic insulator YIG (yttrium iron garnet, $Y_3Fe_5O_{12}$), concludes instead an extremely small $\theta_{SH} = 0.00012$, two orders of magnitude smaller. Both SP experiments have concluded a rather long spin diffusion length λ_{SD} in Bi of 50 nm and 20 nm, respectively.

Remarkably, inserting a thin silver (Ag) layer as NiFe/Ag/Bi substantially enhances both the current and the voltage signals in SP experiments comparing to the signals in NiFe/Bi [24]. The observed signals in NiFe/Ag/Bi cannot be explained using ISHE, thus leading to the proposal of a novel mechanism of spin-to-charge conversion at Bi/Ag Rashba interface [33], namely the inverse Rashba-Edelstein effect (IREE) [34, 35]. Subsequent works have shown similar results in NiFe/Ag/Sb [25] and Fe/Ag/Sn [36] using SP. Moreover, the signals for Ag/Bi/Fe and Bi/Fe have opposite signs [26]. The spin-to-charge conversion efficiency measured in $Ni_{20}Fe_{80}$/Ag/Bi by SP has been shown to be almost independent of temperature [27]. Besides Bi/Ag bilayers [24–29], the IREE has also been explored in other systems, such as surface states of topological insulators (e.g., $Bi_{1.5}Sb_{0.5}Te_{1.7}Se_{1.3}$, Sn-doped Bi_2Te_2Se [23], and α-Sn [36]), two-dimensional electron systems at oxide interfaces (e.g., $LaAlO_3/SrTiO_3$ [37]), and metal/oxide interfaces (e.g., Cu/Bi_2O_3 [38]). These results appear to be consistent with the IREE. The spin-to-charge conversion via the IREE in some materials has been claimed to be more efficient than the ISHE in Pt [36, 37].

However, the overwhelming majority of the IREE studies employ SP with a FM metal (e.g., Fe) as the spin injector [23–27, 36–38]. As concluded by recent SP studies with FM metals, the FMR microwave exciting magnetization dynamics also induces a number of parasitic effects simultaneously [39–42], including the DC electromotive forces due to rf-current rectification via anisotropic magnetoresistance effect, planar Hall effect and anomalous Hall effect. Some such effects manifest with the same symmetry as that of spin-to-charge conversion, thus potentially leading to incorrect interpretations [40, 41].

In this Letter, we report thermally injected spin current transport in Bi films and Bi/Ag bilayers on YIG via LSSE at room temperature. Since YIG is an insulator, several key parasitic effects due to charge carriers in FM metals are absent. We show that pure spin current has been injected into the Bi layer to a depth of several nanometers but leading to *negligible* spin-to-charge conversion and there is no detectable evidence of the IREE at Bi/Ag interfaces. We note Bi is a well-known thermoelectric material that generates large transverse thermovoltages due to the Nernst effect but *unrelated* to

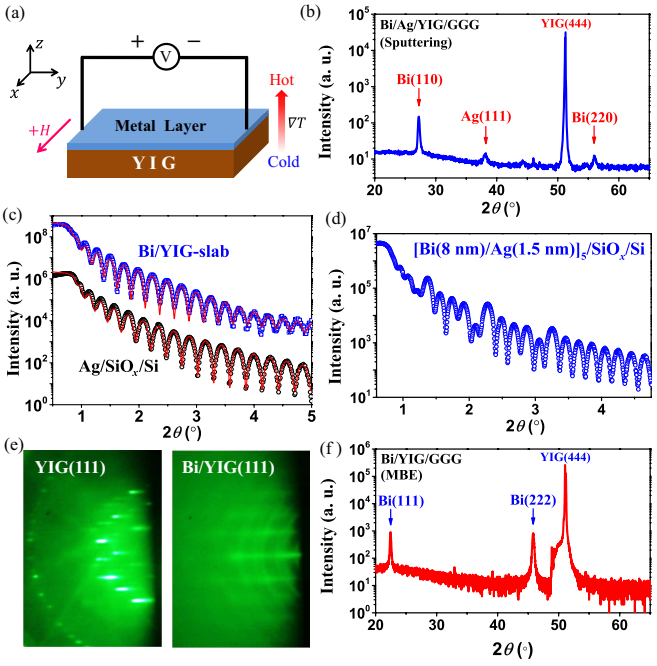

FIG. 1. (a) Schematic diagram for measuring LSSE in metallic thin film/YIG samples. The device dimension is 2 mm×6 mm×0.5 mm. (b) XRD results of Bi(100 nm)/Ag(100 nm)/YIG/GGG grown by low-temperature sputtering. (c) XRR results of low-temperature sputtered Bi(30 nm)/YIG-slab (scaled by a factor of 10^3) and Ag(30 nm)/SiO_x/Si. The red curves are fits to XRR results, indicating that the thickness of Bi(Ag) is 31.6 nm(30.5 nm) and the surface roughness of Bi(Ag) is 0.4 nm(0.5 nm). (d) XRR of the superlattice [Bi(8 nm)/Ag(1.5 nm)]$_5$/SiO_x/Si grown by low-temperature sputtering. (e) RHEED patterns of YIG/GGG substrates and Bi(30 nm)/YIG/GGG samples grown by MBE. (f) XRD results of Bi(60 nm)/YIG/GGG grown by MBE.

spin-to-charge conversion.

The thermal injection scheme is shown in Fig. 1(a). Under an out-of-plane temperature gradient ($\nabla_z T$), the LSSE causes YIG to inject a pure spin current $\boldsymbol{j}_S$ into the adjacent metallic layer. The spin-to-charge conversion via the ISHE in the adjacent metallic layer gives rise to an electric field $\boldsymbol{E}_{ISHE} \propto \boldsymbol{j}_S \times \boldsymbol{\sigma}$ that gives the ISHE voltage, where $\boldsymbol{j}_S$ is the spin current parallel to the temperature gradient $\nabla_z T$ and $\boldsymbol{\sigma}$ is the spin index along the direction of the surface magnetization $\boldsymbol{M}$ of YIG [43]. The thermal injection of spin current by LSSE with a magnetic insulator enjoys the advantages of a simple injection and detection scheme without the complexities due to radio-frequency electromagnetic induction in SP. The LSSE has been rigorously evaluated [12, 13]; metals with positive and negative θ_{SH} gives ISHE voltages of opposite sign [18], and that the ISHE voltage vanishes when the spin current has been blocked by a non-magnetic insulating layer [13, 44].

We used DC magnetron sputtering to deposit Bi and Ag layers onto YIG substrates maintained at liquid nitrogen temperature (∼77 K). Such a low substrate temperature during deposition is used for achieving Bi layers with small roughnesses [45]. We used two types of YIG substrates: 0.5-mm-thick polycrystalline YIG slabs (YIG-slab) and 5-μm-thick single crystalline YIG films liquid-phase-epitaxial on GGG(111) substrates (YIG/GGG). The crystal structures, thicknesses, and roughnesses of the thin-film samples were characterized by X-ray diffraction (XRD) and X-ray reflectivity (XRR) with a Cu K_α radiation. As shown in Fig. 1(b), the Bi layers fabricated by low-temperature sputtering show a preferred orientation along the rhombohedral-(110) direction, as indicated by the prominent Bi(110) and Bi(220) XRD peaks. The Ag layer grows in the cubic crystallography phase with a texture mainly in the (111) direction. The XRR scans reveal thicknesses close to the nominal values [Fig. 1(c)]. In particular, the roughnesses of the Bi and Ag layers are 0.4 nm and 0.5 nm respectively, much smaller than the value of 3.5 nm reported in previous SP works [24]. The interfacial roughness of Bi/Ag in this present work is also relatively small, as indicated by the XRR of the superlattice [Bi(8 nm)/Ag(1.5 nm)]$_5$/SiO_x/Si [Fig. 1(d)] where several characteristic superlattice peaks with a 5-fold oscillating period are observed. Some other layers, such as Pt, W, and MgO, were deposited by sputtering at room temperature without breaking the vacuum. In addition, we have also studied Bi(111) thin films fabricated by room-temperature molecular beam epitaxy (MBE) on the YIG/GGG substrates. The sample quality was characterized *in-situ* using reflection high-energy electron diffraction (RHEED) during growth [Fig. 1(e)], indicating flat and long-range ordered crystal structures at both YIG surfaces and Bi surfaces. The Bi films are nearly single crystalline with the rhombohedral-(111) orientation [Fig. 1(f)].

We performed the LSSE measurements by placing the sample between a Cu block heat sink and a resistance heater to generate an out-of-plane temperature gradient along the z axis. The heat flux was kept constant of 0.06 W/mm^2 with a temperature gradient of about 10 K/mm across the YIG substrates. The transverse thermovoltage along the y axis was measured with an in-plane magnetic field along the x axis [Fig. 1(a)]. The distance between the two voltage leads is about 6 mm.

We first illustrate the LSSE measurements in Pt(3 nm)/YIG-slab [Fig. 2(a)]. This is the well-established LSSE/ISHE result. The ISHE voltage saturates at about 50 mT, which aligns the YIG-slab magnetization. The plateau behavior at low fields ($\leq$ 20 mT) is due to the switching of surface domains in YIG-slab, illustrating that LSSE is sensitive to the surface magnetization [43]. Indeed, the YIG thin film sample of Pt(3 nm)/YIG(5 μm)/GGG has very similar results but does not exhibit such a plateau at low fields [Fig. 2(c)]. After a

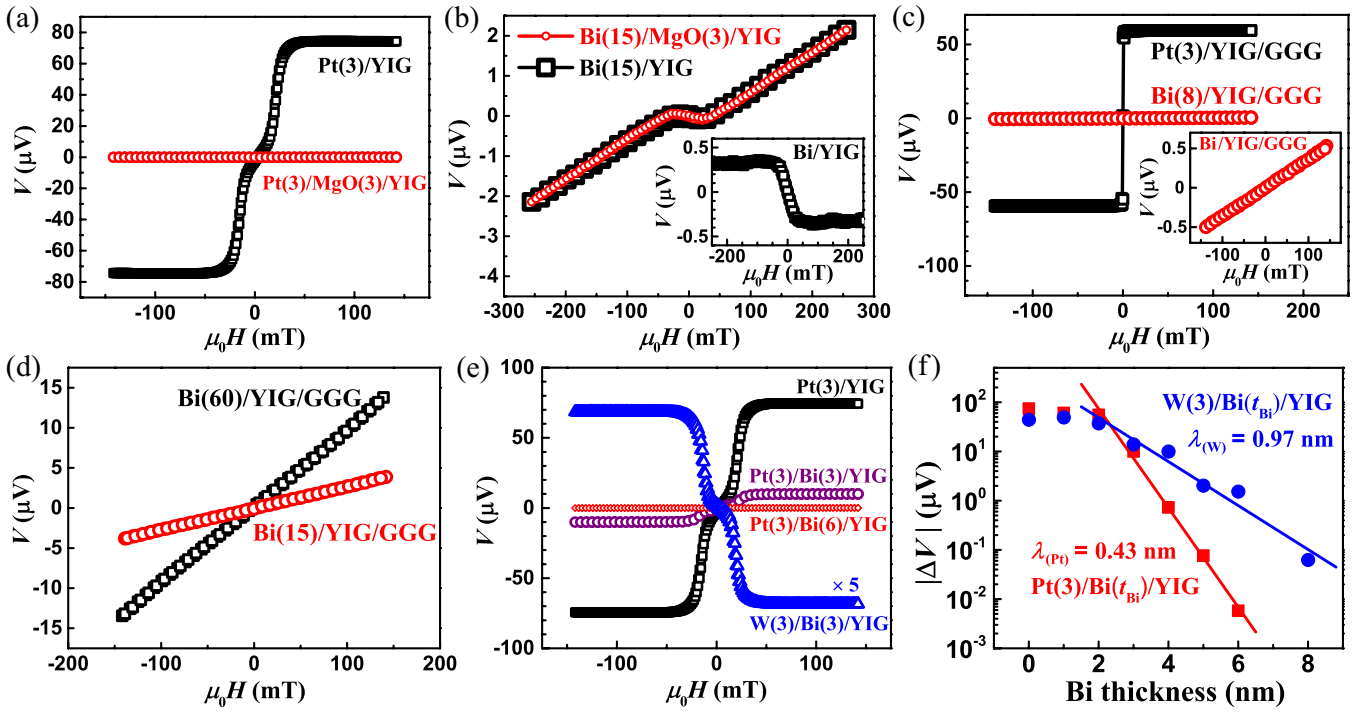

FIG. 2. (a)-(e) Transverse thermovoltages as the function of the in-plane applied magnetic field measured in (a) Pt(3 nm)/YIG-slab and Pt(3 nm)/MgO(3 nm)/YIG-slab, (b) Bi(15 nm)/YIG-slab and Bi(15 nm)/MgO(3 nm)/YIG-slab, (c) Pt(3 nm)/YIG/GGG and Bi(8 nm)/YIG/GGG, (d) Bi(15 nm)/YIG/GGG and Bi(60 nm)/YIG/GGG, (e) Pt(3 nm)/YIG-slab, Pt(3 nm)/Bi(3 nm)/YIG-slab, Pt(3 nm)/Bi(6 nm)/YIG-slab, and W(3 nm)/Bi(3 nm)/YIG-slab (scaled by a factor of 5). Samples in (a)-(c) and (e) are grown by sputtering, whereas those in (d) by MBE. The inset to (b) shows the thermovoltages in Bi(15 nm)/YIG-slab after subtracting a straight line from the raw data. The inset to (c) shows the zoom-in plot of the thermovoltages in Bi(8 nm)/YIG/GGG. (f) The amplitudes of ISHE voltages $|\Delta V|$ in Pt(3 nm)/Bi($t_{\rm Bi}$)/YIG-slab (red squares) and W(3 nm)/Bi($t_{\rm Bi}$)/YIG-slab (blue circles) as the function of $t_{\rm Bi}$. The lines are exponential-decay-function fits to the data ($t_{\rm Bi} \geq 2$ nm) with the effective decay length λ.

MgO(3 nm) layer has been inserted between Pt and YIG-slab, the prominent ISHE signal effect in Pt/YIG vanishes in Pt(3 nm)/MgO(3 nm)/YIG [Fig. 2(a)], demonstrating that the non-magnetic insulating MgO(3 nm) layer completely blocks the spin current. When W instead of Pt has been used, the ISHE voltage reverses sign because of the negative $\theta_{\rm SH}$ of W. These experiments conclusively establish pure spin current phenomena in Pt/YIG under thermal injection.

Diametrically different behavior has been observed in Bi/YIG. As shown in Fig. 2(b), the thermovoltage in the sputtered Bi(15 nm)/YIG-slab increases with the external magnetic field without saturation. Even more surprising, after the insertion of a MgO(3 nm) layer between Bi and YIG, the measured voltages remain *unchanged*. Since the MgO(3 nm) layer should have completely blocked any spin current, the measured voltages in Bi/YIG have nothing to do with spin-to-charge conversion. A small kink at low magnetic field [inset to Fig. 2(b)], which is present in both results of Bi/YIG-slab and Bi/MgO/YIG-slab, reflects reversal of the bulk magnetization in YIG-slab and change of stray fields. Indeed, the results in Bi(8 nm)/YIG/GGG show only the linear dependence on applied magnetic fields without the kink [inset to Fig. 2(c)]. We have also observed the same linear field dependence in Bi(8 nm)/SiO_x/Si under the thermal gradient. In LSSE measurements in Bi/YIG/GGG samples grown by MBE, we have also found no evidence of spin current contribution [Fig. 2(d)]. All of these results unequivocally show the voltages observed in Bi/YIG are unrelated to spin-to-charge conversion; the results are just the ordinary Nernst effect in Bi.

The Nernst effect [46], where the current is driven by a thermal gradient, is the thermal analogue of the Hall effect. The electric field of Nernst effect due to the thermally driven charge current in a magnetic field is $\boldsymbol{E}_{\rm NE} \propto \nabla T \times \boldsymbol{B}$. Note that the Nernst effect is scaled with the $\boldsymbol{B}$-field, while the LSSE in Pt/YIG is scaled with the surface magnetization $\boldsymbol{M}$ of YIG. The Nernst effect is negligible in common metals, such as Ag and Pt, but orders of magnitude larger in Bi due to the small Fermi energy and large electron mobility [47]. Indeed, the Nernst effect was discovered in Bi, which has the largest known Nernst coefficient among elemental metals [47]. Even when the mobility in Bi thin films is limited by

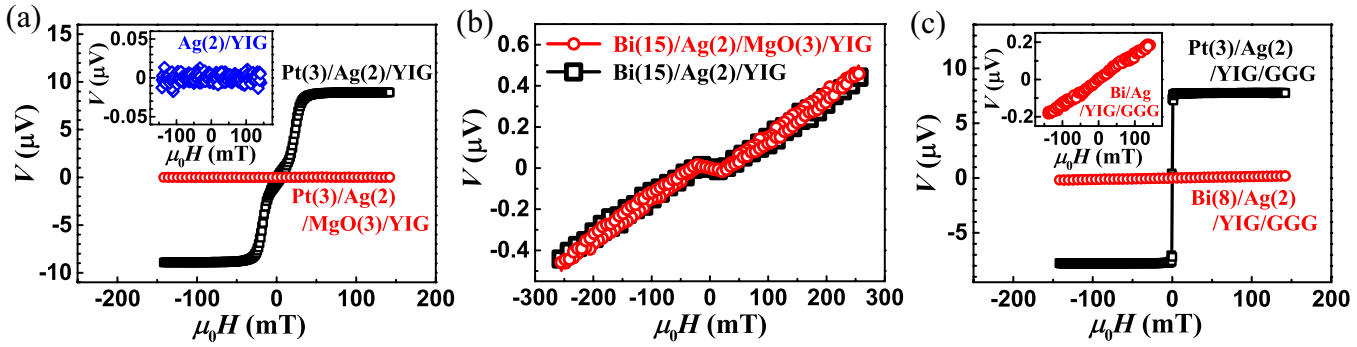

FIG. 3. Transverse thermovoltages as the function of the in-plane external magnetic field measured in (a) Pt(3 nm)/Ag(2 nm)/YIG-slab, Pt(3 nm)/Ag(2 nm)/MgO(3 nm)/YIG-slab, and Ag(2 nm)/YIG-slab in the inset, (b) Bi(15 nm)/Ag(2 nm)/YIG-slab and Bi(15 nm)/Ag(2 nm)/MgO(3 nm)/YIG-slab, (c) Pt(3 nm)/Ag(2 nm)/YIG/GGG and Bi(8 nm)/Ag(2 nm)/YIG/GGG. The inset to (c) shows the zoom-in plot of the thermovoltages in Bi(8 nm)/Ag(2 nm)/YIG/GGG.

the surface scattering, the more modest Nernst voltage remains substantial and comparable to the ISHE voltage in Pt/YIG [Fig. 2(d)]. In addition to the different field dependence, the Nernst signal in Bi films increases with thickness in the studied range ($t_{\rm Bi} < 100$ nm), whereas the LSSE signal in Pt/YIG decreases with increasing Pt thickness limited by the spin diffusion length [18].

We have found no evidence of spin current contribution in Bi/YIG. The key question is whether the spin current has been injected into the Bi layer at all. To address this question, we have measured Pt(3 nm)/Bi($t_{\rm Bi}$)/YIG and W(3 nm)/Bi($t_{\rm Bi}$)/YIG, designed to detect the emergent spin current through the Bi layer by Pt and W respectively. As shown in Fig. 2(e), we have observed the spin-to-charge signals in Pt(3 nm)/Bi(3 nm)/YIG and W(3 nm)/Bi(3 nm)/YIG samples with opposite signs due to the different signs of $\theta_{\rm SH}$ in Pt and W. These signals are those of ISHE from spin current that has passed through the Bi layer and converted in the Pt and W layers. Thus, we have demonstrated that the pure spin current has been injected via LSSE from YIG into Bi, and has passed through the Bi layer, but with negligibly small spin-to-charge conversion within Bi. The value of $\theta_{\rm SH}$ in Bi cannot be larger than 2×10^{-5} (see Supplemental Material). The signal in the Pt(3 nm)/Bi($t_{\rm Bi}$)/YIG trilayer gradually decreases with increasing $t_{\rm Bi}$ and becomes barely detectable in Pt(3 nm)/Bi(6 nm)/YIG [Fig. 2(e)]. In Fig. 2(f), we show the amplitudes of the ISHE voltages $|\Delta V|$ in the Pt(3 nm)/Bi($t_{\rm Bi}$)/YIG and the W(3 nm)/Bi($t_{\rm Bi}$)/YIG trilayers as a function of $t_{\rm Bi}$. We find that for 2 nm $\leq t_{\rm Bi} \leq$ 8 nm, $|\Delta V|$ decays exponentially as $|\Delta V(t_{\rm Bi})| \propto \exp(-t_{\rm Bi}/\lambda)$ with the effective decay length λ of about 0.43 nm in Pt(3 nm)/Bi($t_{\rm Bi}$)/YIG and about 0.97 nm in W(3 nm)/Bi($t_{\rm Bi}$)/YIG. These values are in sharp contrast to the previously reported very long spin diffusion length $\lambda_{\rm SD}$ in Bi (50 nm or 20 nm) at room temperature [19, 20], but closer to the small $\lambda_{\rm SD}$ of 0.11 nm at Bi/Cu interfaces reported by the recent LSV experiments [32]. For $t_{\rm Bi} \leq 2$ nm, the ISHE voltages deviate from the exponential behavior [48].

We next describe spin injection into Bi/Ag bilayers by LSSE in YIG-slab. As shown in Fig. 3(a), the LSSE is readily observable in Pt(3 nm)/Ag(2 nm)/YIG but not in Pt(3 nm)/Ag(2 nm)/MgO(3 nm)/YIG when the spin current has been blocked by the MgO(3 nm) layer. The Ag layer has negligibly small LSSE contribution because of its small $\theta_{\rm SH}$, as shown by the results of Ag(2 nm)/YIG [inset to Fig. 3(a)]. The LSSE signal in Pt/Ag/YIG results from spin currents passing through the Ag layer and then converting into charge signals by ISHE in the Pt layer. Completely different behaviors have been observed in Bi(15 nm)/Ag(2 nm)/YIG and Bi(15 nm)/Ag(2 nm)/MgO(3 nm)/YIG, both of which show the same voltages [Fig. 3(b)]. These results indicate conclusively that the magneto-thermoelectric signals in Bi/Ag/YIG have nothing to do with spin current. We have also studied the layer structures with YIG thin films of Pt(3 nm)/Ag(2 nm)/YIG/GGG [Fig. 3(c)], which show clear evidence of spin-to-charge conversion as those in Fig. 3(a), except the surface domain switching at small fields. But the results of Bi/Ag/YIG/GGG are totally different [inset to Fig. 3(c)]. These results, linearly dependent on applied magnetic fields and with no correlation to the magnetization of YIG, are simply due to the Nernst effect in the Bi layer. Since the spin current definitely reaches the Bi/Ag interface, the lack of spin-to-charge signals in Bi/Ag bilayers indicates the absence of spin-to-charge conversion at the Bi/Ag interface.

We have also studied Bi films and Bi/Ag bilayers thermally evaporated on YIG/GGG substrates (see Supplemental Material). The evaporated Bi film is polycrystalline with (111) and (110) texture and the roughness of about 2 nm. The transverse thermovoltages in the evaporated Bi(8 nm)/YIG/GGG and Bi(8 nm)/Ag(5 nm)/YIG/GGG, are proportional to the in-plane applied magnetic field, indicating the Nernst effect in the Bi layer. There is no detectable spin-to-charge

signal in the thermally evaporated Bi films and Bi/Ag bilayers. These thermally evaporated samples have comparable roughness to the prior report [24] but still show no IREE, suggesting that neither sharp nor rough (alloyed) Bi/Ag interface yields notable spin-to-charge conversion.

Despite being a heavy element with strong SOC, we have shown that Bi has negligible spin-to-charge conversion despite previous claims to the contrary. This may be surprising at first glance. However, we note the well-known heavy elements with large θ_{SH} (Pt, W, Ta, etc.) are d-orbital elements. Those with less than (more than) half full d shell have positive (negative) θ_{SH} [17, 18]. Thus the electronic configuration, rather than the detailed band structures of the materials, dominates the intrinsic spin Hall effect [16]. Bi is a p-orbital element with unfilled $6p$ shell. We conjecture that p-shell elements exhibit poor spin-to-charge conversion characteristics. This can be more rigorously tested experimentally by exploring other p-shell elements, such as Pb and Sb.

In summary, we have investigated the spin-to-charge conversion in Bi films and Bi/Ag bilayers via LSSE at room temperature. Despite the large spin-orbit interaction in Bi and the strong Rashba spin-splitting at Bi/Ag interfaces, we have not found appreciable spin-to-charge conversion signals in the Bi films and the Bi/Ag bilayers. Instead, there are substantial magneto-thermoelectric effects simply due to the ordinary Nernst effect in Bi with a linear dependence on magnetic field. The results lack evidence of spin-to-charge conversion at the Bi/Ag interface, thus the present understanding of the IREE need more careful evaluation.

This work was supported by the U.S. Department of Energy, Office of Science, Basic Energy Science (Grant No. DE-SC0009390), the National Basic Research Program of China (Grants No. 2015CB921402 and No. 2011CB921802), and the National Science Foundation of China (Grants No. 11374057, No. 11434003, and No. 11421404).

[1] N. F. Mott, "The scattering of fast electrons by atomic nuclei," Proc. R. Soc. A **124**, 425–442 (1929).
[2] M. I. Dyakonov and V. I. Perel, "Possibility of orienting electron spins with current," JETP Letters **13**, 467–469 (1971).
[3] J. E. Hirsch, "Spin Hall effect," Phys. Rev. Lett. **83**, 1834–1837 (1999).
[4] P. Monod, H. Hurdequint, A. Janossy, J. Obert, and J. Chaumont, "Giant electron spin-resonance transmission in Cu ion implanted with Mn," Phys. Rev. Lett. **29**, 1327–1330 (1972).
[5] R. H. Silsbee, A. Janossy, and P. Monod, "Coupling between ferromagnetic and conduction-spin-resonance modes at a ferromagnetic–normal-metal interface," Phys. Rev. B **19**, 4382–4399 (1979).
[6] Y. Tserkovnyak, A. Brataas, and Gerrit E. W. Bauer, "Enhanced Gilbert damping in thin ferromagnetic films," Phys. Rev. Lett. **88**, 117601 (2002).
[7] E. Saitoh, M. Ueda, H. Miyajima, and G. Tatara, "Conversion of spin current into charge current at room temperature: Inverse spin-Hall effect," Appl. Phys. Lett. **88**, 182509 (2006).
[8] M. V. Costache, M. Sladkov, S. M. Watts, C. H. van der Wal, and B. J. van Wees, "Electrical detection of spin pumping due to the precessing magnetization of a single ferromagnet," Phys. Rev. Lett. **97**, 216603 (2006).
[9] Y. Kajiwara, K. Harii, S. Takahashi, J. Ohe, K. Uchida, M. Mizuguchi, H. Umezawa, H. Kawai, K. Ando, K. Takanashi, S. Maekawa, and E. Saitoh, "Transmission of electrical signals by spin-wave interconversion in a magnetic insulator," Nature (London) **464**, 262 (2010).
[10] M. Johnson and R. H. Silsbee, "Interfacial charge-spin coupling: Injection and detection of spin magnetization in metals," Phys. Rev. Lett. **55**, 1790–1793 (1985).
[11] F. J. Jedema, A. T. Filip, and B. J. van Wees, "Electrical spin injection and accumulation at room temperature in an all-metal mesoscopic spin valve," Nature (London) **410**, 345–348 (2001).
[12] K. Uchida, H. Adachi, T. Ota, H. Nakayama, S. Maekawa, and E. Saitoh, "Observation of longitudinal spin-Seebeck effect in magnetic insulators," Appl. Phys. Lett. **97**, 172505 (2010).
[13] T. Kikkawa, K. Uchida, Y. Shiomi, Z. Qiu, D. Hou, D. Tian, H. Nakayama, X.-F. Jin, and E. Saitoh, "Longitudinal spin Seebeck effect free from the proximity Nernst effect," Phys. Rev. Lett. **110**, 067207 (2013).
[14] S. M. Rezende, R. L. Rodríguez-Suárez, R. O. Cunha, A. R. Rodrigues, F. L. A. Machado, G. A. Fonseca Guerra, J. C. Lopez Ortiz, and A. Azevedo, "Magnon spin-current theory for the longitudinal spin-Seebeck effect," Phys. Rev. B **89**, 014416 (2014).
[15] N. S. Averkiev and M. I. Dyakonov, "Current due to inhomogeneity of the spin orientation of electrons in a semiconductor," Sov. Phys. Semicond. **17**, 393–395 (1983).
[16] T. Tanaka, H. Kontani, M. Naito, T. Naito, D. S. Hirashima, K. Yamada, and J. Inoue, "Intrinsic spin Hall effect and orbital Hall effect in $4d$ and $5d$ transition metals," Phys. Rev. B **77**, 165117 (2008).
[17] M. Morota, Y. Niimi, K. Ohnishi, D. H. Wei, T. Tanaka, H. Kontani, T. Kimura, and Y. Otani, "Indication of intrinsic spin Hall effect in $4d$ and $5d$ transition metals," Phys. Rev. B **83**, 174405 (2011).
[18] D. Qu, S. Y. Huang, B. F. Miao, S. X. Huang, and C. L. Chien, "Self-consistent determination of spin Hall angles in selected $5d$ metals by thermal spin injection," Phys. Rev. B **89**, 140407 (2014).
[19] D. Hou, Z. Qiu, K. Harii, Y. Kajiwara, K. Uchida, Y. Fujikawa, H. Nakayama, T. Yoshino, T. An, K. Ando, X. Jin, and E. Saitoh, "Interface induced inverse spin Hall effect in bismuth/permalloy bilayer," Appl. Phys. Lett. **101**, 042403 (2012).
[20] H. Emoto, Y. Ando, G. Eguchi, R. Ohshima, E. Shikoh, Y. Fuseya, T. Shinjo, and M. Shiraishi, "Transport and spin conversion of multicarriers in semimetal bismuth," Phys. Rev. B **93**, 174428 (2016).
[21] Y. Niimi, Y. Kawanishi, D. H. Wei, C. Deranlot, H. X. Yang, M. Chshiev, T. Valet, A. Fert, and Y. Otani, "Giant spin Hall effect induced by skew scattering

from bismuth impurities inside thin film CuBi alloys," Phys. Rev. Lett. **109**, 156602 (2012).
[22] A. R. Mellnik, J. S. Lee, A. Richardella, J. L. Grab, P. J. Mintun, M. H. Fischer, A. Vaezi, A. Manchon, E. A. Kim, N. Samarth, and D. C. Ralph, "Spin-transfer torque generated by a topological insulator," Nature (London) **511**, 449 (2014).
[23] Y. Shiomi, K. Nomura, Y. Kajiwara, K. Eto, M. Novak, K. Segawa, Y. Ando, and E. Saitoh, "Spin-electricity conversion induced by spin injection into topological insulators," Phys. Rev. Lett. **113**, 196601 (2014).
[24] J.-C. Rojas-Sánchez, L. Vila, G. Desfonds, S. Gambarelli, J. P. Attané, J. M. De Teresa, C. Magén, and A. Fert, "Spin-to-charge conversion using Rashba coupling at the interface between non-magnetic materials," Nat. Commun. **4**, 2944 (2013).
[25] W. Zhang, M. B. Jungfleisch, W. Jiang, J. E. Pearson, and A. Hoffmann, "Spin pumping and inverse Rashba-Edelstein effect in NiFe/Ag/Bi and NiFe/Ag/Sb," J. Appl. Phys. **117**, 17C727 (2015).
[26] S. Sangiao, J. M. De Teresa, L. Morellon, I. Lucas, M. C. Martinez-Velarte, and M. Viret, "Control of the spin to charge conversion using the inverse Rashba-Edelstein effect," Appl. Phys. Lett. **106**, 172403 (2015).
[27] A. Nomura, T. Tashiro, H. Nakayama, and K. Ando, "Temperature dependence of inverse Rashba-Edelstein effect at metallic interface," Appl. Phys. Lett. **106**, 212403 (2015).
[28] M. Matsushima, Y. Ando, S. Dushenko, R. Ohshima, R. Kumamoto, T. Shinjo, and M. Shiraishi, "Quantitative investigation of the inverse Rashba-Edelstein effect in Bi/Ag and Ag/Bi on YIG," Appl. Phys. Lett. **110**, 072404 (2017).
[29] H. Nakayama, Y. Kanno, H. An, T. Tashiro, S. Haku, A. Nomura, and K. Ando, "Rashba-Edelstein magnetoresistance in metallic heterostructures," Phys. Rev. Lett. **117**, 116602 (2016).
[30] M. B. Jungfleisch, W. Zhang, J. Sklenar, W. Jiang, J. E. Pearson, J. B. Ketterson, and A. Hoffmann, "Interface-driven spin-torque ferromagnetic resonance by Rashba coupling at the interface between nonmagnetic materials," Phys. Rev. B **93**, 224419 (2016).
[31] H. J. Zhang, S. Yamamoto, B. Gu, H. Li, M. Maekawa, Y. Fukaya, and A. Kawasuso, "Charge-to-spin conversion and spin diffusion in Bi/Ag bilayers observed by spin-polarized positron beam," Phys. Rev. Lett. **114**, 166602 (2015).
[32] M. Isasa, M. C. Martínez-Velarte, E. Villamor, C. Magén, L. Morellón, J. M. De Teresa, M. R. Ibarra, G. Vignale, E. V. Chulkov, E. E. Krasovskii, L. E. Hueso, and F. Casanova, "Origin of inverse Rashba-Edelstein effect detected at the Cu/Bi interface using lateral spin valves," Phys. Rev. B **93**, 014420 (2016).
[33] C. R. Ast, J. Henk, A. Ernst, L. Moreschini, M. C. Falub, D. Pacilé, P. Bruno, K. Kern, and M. Grioni, "Giant spin splitting through surface alloying," Phys. Rev. Lett **98**, 186807 (2007).
[34] V. M. Edelstein, "Spin polarization of conduction electrons induced by electric current in two-dimensional asymmetric electron systems," Solid State Commun. **73**, 233–235 (1990).
[35] N. S. Averkiev and I. A. Kokurin, "Current-induced spin orientation in semiconductors and low-dimensional structures," J. Magn. Magn. Mater. **440**, 157–160 (2017).
[36] J.-C. Rojas-Sánchez, S. Oyarzún, Y. Fu, A. Marty, C. Vergnaud, S. Gambarelli, L. Vila, M. Jamet, Y. Ohtsubo, A. Taleb-Ibrahimi, P. Le Fèvre, F. Bertran, N. Reyren, J.-M. George, and A. Fert, "Spin to charge conversion at room temperature by spin pumping into a new type of topological insulator: α-Sn films," Phys. Rev. Lett. **116**, 096602 (2016).
[37] E. Lesne, Yu Fu, S. Oyarzun, J.-C. Rojas-Sánchez, D. C. Vaz, H. Naganuma, G. Sicoli, J.-P. Attané, M. Jamet, E. Jacquet, J.-M. George, A. Barthélémy, H. Jaffrès, A. Fert, M. Bibes, and L. Vila, "Highly efficient and tunable spin-to-charge conversion through Rashba coupling at oxide interfaces," Nat. Mater. **15**, 1261 (2016).
[38] S. Karube, K. Kondou, and Y. Otani, "Experimental observation of spin-to-charge current conversion at non-magnetic metal/Bi_2O_3 interfaces," Appl. Phys. Express **9**, 033001 (2016).
[39] W. G. Egan and H. J. Juretschke, "DC detection of ferromagnetic resonance in thin nickel films," J. Appl. Phys. **34**, 1477–1484 (1963).
[40] M. Harder, Y. Gui, and C.-M. Hu, "Electrical detection of magnetization dynamics via spin rectification effects," Phys. Rep. **661**, 1–59 (2016).
[41] R. Iguchi and E. Saitoh, "Measurement of spin pumping voltage separated from extrinsic microwave effects," J. Phys. Soc. Jpn. **86**, 011003 (2017).
[42] S. Keller, J. Greser, M. R. Schweizer, A. Conca, V. Lauer, C. Dubs, B. Hillebrands, and E. Th. Papaioannou, "Relative weight of the inverse spin-Hall and spin-rectification effects for metallic polycrystalline Py/Pt, epitaxial Fe/Pt, and insulating YIG/Pt bilayers: Angular dependent spin pumping measurements," Phys. Rev. B **96**, 024437 (2017).
[43] P.-H. Wu and S.-Y. Huang, "Noncollinear magnetization between surface and bulk $Y_3Fe_5O_{12}$," Phys. Rev. B **94**, 024405 (2016).
[44] W. Lin, K. Chen, S. Zhang, and C. L. Chien, "Enhancement of thermally injected spin current through an antiferromagnetic insulator," Phys. Rev. Lett. **116**, 186601 (2016).
[45] K. S. Wu and M. Y. Chern, "Electrical transport properties of n-type (110)-oriented bismuth thin films grown at 110 K on glass substrates," J. Appl. Phys. **104**, 033704 (2008).
[46] H. J. Goldsmid, *Introduction to Thermoelectricity*, Springer Series in Materials Science (Springer-Verlag Berlin Heidelberg, 2016).
[47] K. Behnia and H. Aubin, "Nernst effect in metals and superconductors: a review of concepts and experiments," Rep. Prog. Phys. **79**, 046502 (2016).
[48] See Supplemental Material at http://XXX, which includes Refs. [14, 18, 20, 24, 49], for extended data of square resistances R_S and ISHE currents $|\Delta V|/R$ in Pt/Bi/YIG and W/Bi/YIG.
[49] C. Du, H. Wang, F. Yang, and P. C. Hammel, "Enhancement of pure spin currents in spin pumping $Y_3Fe_5O_{12}$/Cu/Metal trilayers through spin conductance matching," Phys. Rev. Applied **1**, 044004 (2014).